Journal of Inorganic and Organometallic Polymers and Materials (2019) 29:402–415
https://doi.org/10.1007/s10904-018-1010-9

Electrical Properties of Cerium and Yttrium Co-substituted Strontium Nanohexaferrites

M. A. Almessiere[1,3] · B. Unal[2] · A. Baykal[3] · I. Ercan[4]

Received: 26 September 2018 / Accepted: 21 October 2018 / Published online: 24 October 2018

Abstract

Ce and Y substituted $SrFe_{12}O_{19}$ (x = 0.4 and 0.5) nanohexaferrites have been synthesised by sol–gel auto-combustion. The pure hexagonal $SrFe_{12}O_{19}$ phase was confirmed by XRD, FE-SEM and HR-TEM. The *ac* conductivity and dielectric properties of Ce and Y substituted Sr:$Fe_{12}O_{19}$ nanohexaferrites were studied by using complex impedance technique. Dielectric properties such as dielectric constant, dielectric loss, dielectric tangent loss, as well as *ac* conductivity are measured at various bias potentials in a varying frequency range from 10 Hz to 10 MHz. The frequency dependency of the *ac* conductivity could be evaluated by a power exponent law at higher frequencies, which is a characteristic mechanism for electrical charge transport by tunnelling processes with which it is more dispersive at lower frequencies. The conduction mechanisms were also investigated at various *dc* bias potentials, mainly being an indicative of hopping type conduction. So, the dielectric dispersion behaviour can be well elucidated in terms of Maxwell–Wagner polarization in accordance with the Koop's phenomenological theory. Utilizing an electrical equivalent circuit model, impedance studies were carried out in a specific frequency domain to characterize all the contributions of the dielectric response between the grains and grain boundaries to the dielectric parameters.

Keywords Sr nanohexaferrite · X-ray diffraction (XRD) · Conductivity · Dielectric loss · Electric modulus

1 Introduction

Magneto plumbite strontium hexaferrites are excellent hard ferrite materials due to their high magnetic coercivity, high chemical stability, high Curie temperature, high electrical resistivity and low-cost production. These properties lead to use in extensively in the recording media, permanent magnets, microwave components, high frequency and magneto optical devices [1, 2]. The magnetic, electrical and dielectric properties can be controlled and adjusted by partial substitution of Fe^{3+} via external ions [3, 4]. Electrical transport and dielectric performances in M-type hexaferrites are powerfully linked with the transferring electrons between Fe^{2+} to Fe^{3+} at B sites, also the resistivity ρ, drift mobility μ, dielectric coefficient ε, and dielectric loss tanδ are ascribed to the phase change and type of substitution ions and the occupation site [5, 6]. Moreover, the *ac* conductivity showed a valued feature about the localized charge carriers and conduction mechanism. This dielectric performance of M-type hexaferrites can be employed for device applications. Many reports have been made on partial substitutions M-type hexaferrite by rare earth ions and other cations for getting the desired magnetic and electric properties such as La^{3+}, Ce^{3+}, Nd^{3+}, [7–9], La–Co [10], La–Ni [11], Nd–Co [12], Ce–Co [13], Gd–Sn [14].

In this study, the structural and dielectric properties of Ce–Y substituted strontium nanohexaferrites (x = 0.4 and 0.5) have been investigated in detail. It also presents valuable information about dielectric properties (dielectric constant,

✉ M. A. Almessiere
malmessiere@iau.edu.sa

1 Department of Physics, College of Science, Imam Abdulrahman Bin Faisal University, P.O. Box 1982, Dammam 31441, Saudi Arabia

2 Department of Software and Computer Engineering, Istanbul Sabahattin Zaim University, Halkali Cad. No: 2, 34303 Halkali-Kucukcekmece, Istanbul, Turkey

3 Department of Nanomedicine Research, Institute for Research & Medical Consultations (IRMC), Imam Abdulrahman Bin Faisal University, P.O. Box 1982, Dammam 31441, Saudi Arabia

4 Department of Physics, Institute for Research & Medical Consultations (IRMC), Imam Abdulrahman Bin Faisal University, P.O. Box 1982, Dammam 31441, Saudi Arabia

dielectric loss, *ac* conductivity and permeability) of this nanohexaferrite material.

2 Experimental

Substituted strontium nanohexaferrites with Ce–Y (x = 0.4 and 0.5) were prepared via sol–gel auto-combustion method. The stoichiometric of amount of strontium nitrate $Sr(NO_3)_2$ (99.9%), iron nitrate extra pure $Fe(NO_3)_3$, cerium nitrate $Ce(NO_3)_2$ (99.9%) were dissolved in 50 ml DI H_2O and Y_2O_3 (99.99%) was dissolved in 10 ml of HCl with stirring at 200 °C till the both solutions becomes transparent. 3 g citric acid was also dissolved in 20 ml DI H_2O under stirring. These three solutions were mixed into one and its pH has been adjusted to 7 via NH_3 soln. dropwise, the temperature was increased to 150 °C for 30 min then 320 °C for 2 h. The resulted powder was calcinated at 1100 °C for 5 h. The details of the synthesis have already been given in our previous publication [15]. The phase identification was executed through Rigaku Benchtop Miniflex X-ray powder diffraction (XRD) with Cu Kα (20°–70°) at room temperature (RT). The morphology, microstructure and chemical analysis were taken via a FEI Titan S/TEM microscope operating up to 300 kV coupled with an EDXS Si(Li) detector. The dielectric measurements are held by Novocontrol Technologies, Alpha-AN with frequency range of 3 μHz–20 MHz.

3 Results and Discussions

3.1 Phase Analysis

Figure 1 presented XRD powder patterns of $SrY_xCe_xFe_{12-2x}O_{19}$ nanohexaferrites (x = 0.4 and 0.5). Match3 Refinement! Program matches the XRD peaks perfectly with Sr hexaferrite phase (card number 96-100-8857). The samples showed absences of any second phase. The lattice parameters 'a' are 5.8821, 5.8972 and 'c' are 23.0230, 23.0945 respectively. The increase in lattice parameters are caused by the ionic radii of Sr^{2+} (1.32 Å), Fe^{3+} (0.78 Å), Ce^{3+} (1.05 Å) and Y^{3+} (0.9 Å) and the amounts of substituted ions. The details of the XRD analysis are given in ref [15].

3.2 Morphology

Figure 2 depicted the micrograph images of $SrY_xCe_xFe_{12-2x}O_{19}$ nanohexaferrites (x = 0.4 and 0.5). The images revealed plate like structure with hexagonal shape that is confirmed the M-type hexaferrite structure. The particles showed aggregation when increasing the amount of substitution ions. The elemental mapping spectra illustrated

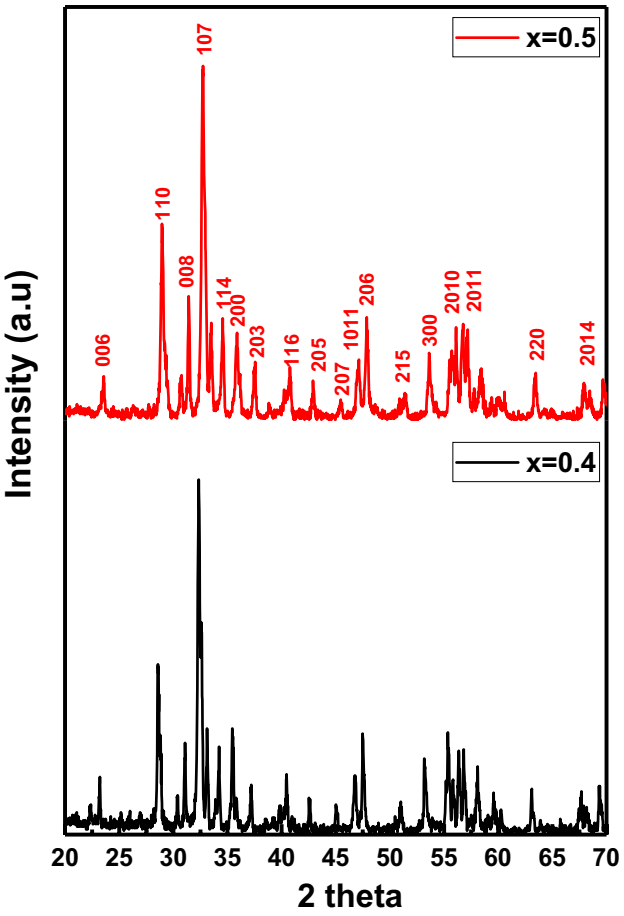

Fig. 1 XRD powder patterns of $SrY_xCe_xFe_{12-2x}O_{19}$ (x = 0.4 and 0.5) nanohexaferrites

the existence elements in composition. In addition, M type hexagonal atomic planes have been proved using HRTEM by calculating the interplanar distance as seen in Fig. 3. The measurements displayed 0.11, 0.12, 0.15, 0.18, 0.20, 0.24, 0.26, 0.28 and 0.3 corresponding to (410), (406), (307), (209), (207), (203), (114), (112) and (106) planes respectively (Table 1).

3.3 Electrical Properties

It is well known that complex impedance spectroscopy is now a powerful tool for investigating dielectric relaxation processes in microstructured polycrystalline specimens [5].

The effects of both Ce and Y ions substituted Sr-hexaferrites on *ac*/*dc* conductivities, dielectric constant, loss mechanism and complex dielectric modulus were extensively investigated for both substitution ratios of 0.4 and 0.5. It has been observed that the *ac* conductivity of Sr-hexaferrites slightly increases as both substitutions increase, as shown in Fig. 4a–d. Moreover, the *ac* conductivity increases as the

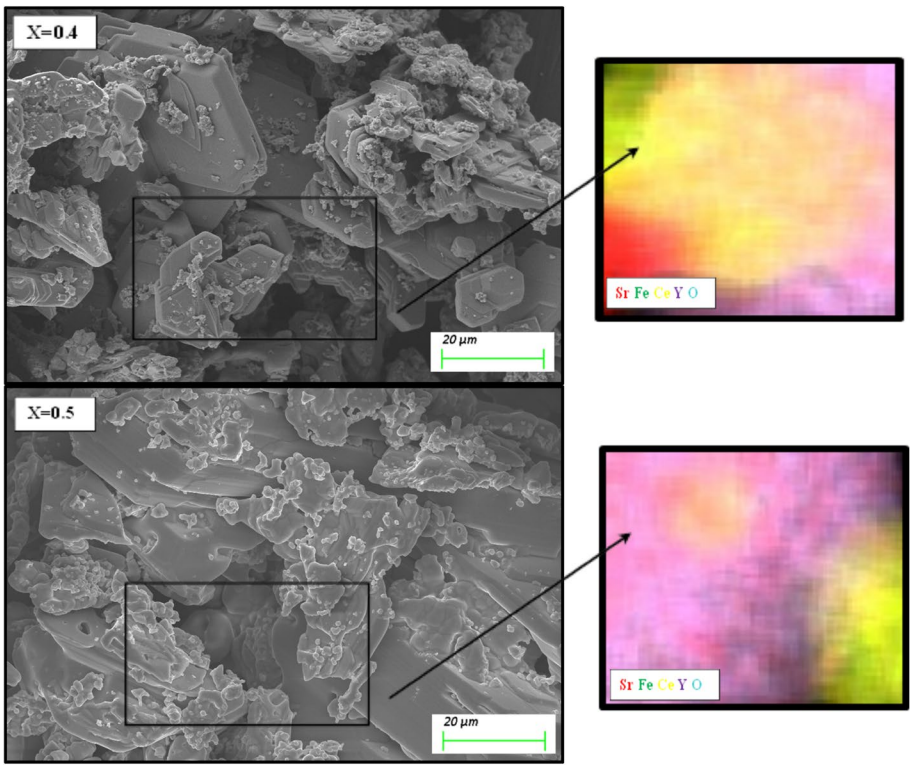

Fig. 2 FE-SEM images and elemental mapping spectra of $SrY_xCe_xFe_{12-2x}O_{19}$ (x = 0.4 and 0.5) nanohexaferrites

frequency increases as an indication of both electronic and polaron hopping mechanism.

So the electrical conduction mechanism of the M-type hexaferrite can solely be interpreted on the basis of the association of ferrous ions with ferric ions situating at adjacent octahedral sites. This leads to a higher conductivity as an interchange ("hopping") of electrons. In addition, the RT conduction of ferrites can be a consequence of impurities. However, the high temperature conduction is a consequence of hopping mechanism. The characteristic trends of both C- and Y-substituted M-type Sr-hexaferrites reveal the dependence of complex dielectric properties on the stimulation frequency, *dc* bias potential basis and substitution rates. As the stimulation frequency increases, the dielectric constant (ε′), dielectric loss (ε″) and dielectric loss tangent (δ) all decreases rapidly. So, the observed mechanism is ascribed to Maxwell–Wagner polarization and conduction mechanism.

In case of ionic hexaferrite, the conduction is -also called "hopping" -mainly owing to the transfer of charge carriers between ferrous and ferric cations in the different valance states. The conductivity under the electron jump effect exhibits some typical semiconductor properties resulting from the behavior of the different carriers shown at different *dc* bias potentials.

The *ac* conductivity measurements of $SrY_xCe_xFe_{12-2x}O_{19}$ nanohexaferrites (x = 0.4 and 0.5) were carried out in the range of 10 Hz–10 MHz for *dc* bias potentials between − 10 and 10 V using impedance spectroscopy for both substitutional ratios. The frequency dependency of conductivity at different bias potentials can be represented in Fig. 4. It is clearly noticed that some polarity independence is observed in the *dc* polarity variations at low frequencies while there is no significant change in *ac* conductivity at high frequencies. The *dc* bias potentials, ranging from − 10 to + 10 V, have no significant effect on the *ac* conductivity, especially at higher frequencies, while at lower frequencies the nearly symmetrical tendency will have various effects (see Fig. 4a, b). It is also observed that the *ac* conductivity increases with increasing frequency (see Fig. 4c, d). Possible mechanism responsible for this phenomenon can be due to the electrons hopping between ferric and ferrous ions at octahedral sites. This causes an increase in the hopping of charge carriers between cations having different valance states of ferric and ferrous ions. At lower frequencies this type of dispersion in conductivity is attributable to the existence of grain boundaries, while the consistency in higher frequency region is due to the conducting grains. So, another reason for low-frequency dispersion in the hexaferrites can be observed depending on a space-charge effect. Furthermore, the interfacial density of states in the microstructured hexaferrites could act as charge carriers owing to ionization, thus might be functionalized as conduction centers supporting the transference of charge carriers as well. At the same time, it was concluded that the conductivity of both substituted Sr-hexaferrites is a linear

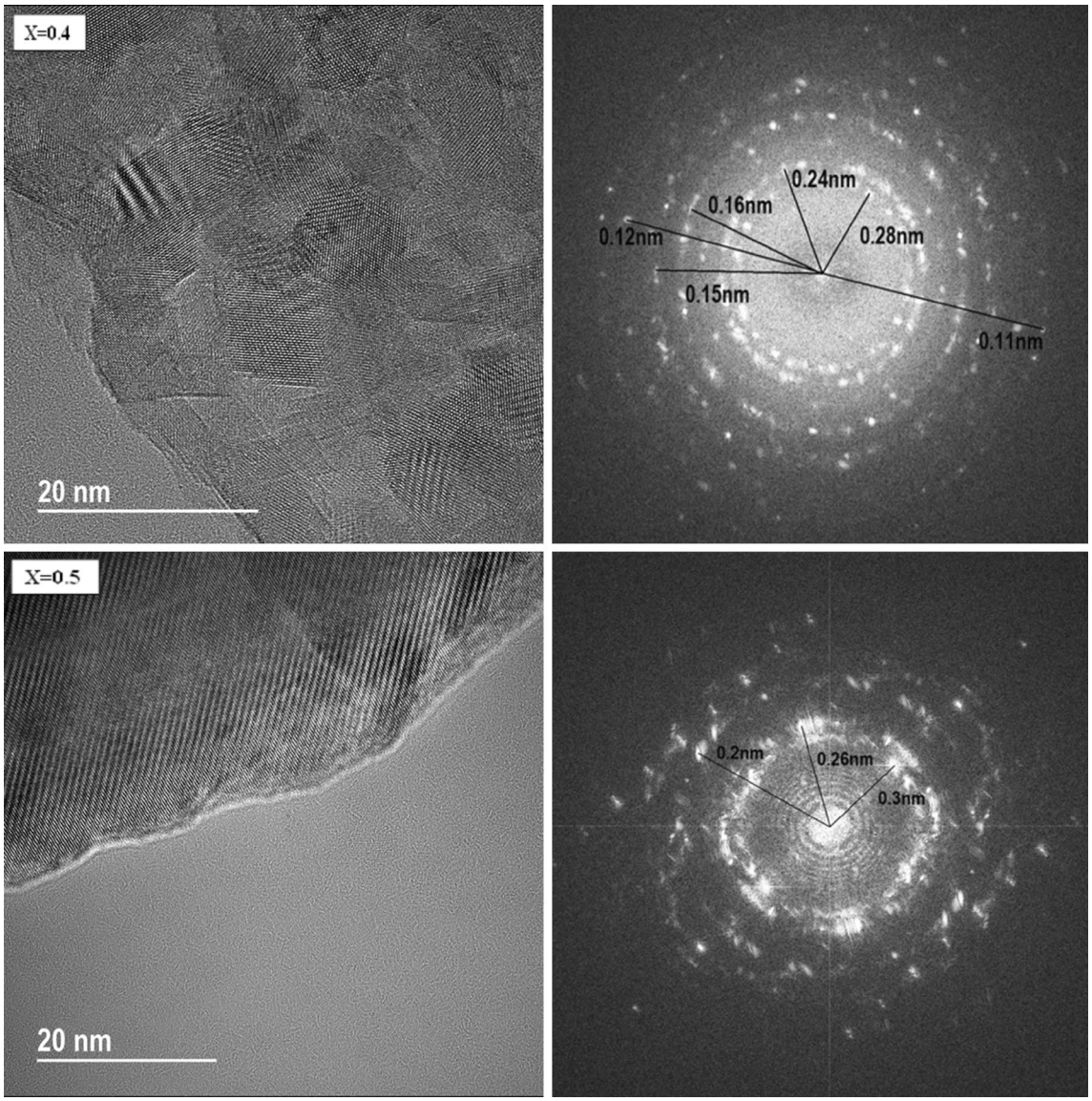

Fig. 3 HR-TEM image of $SrY_xCe_xFe_{12-2x}O_{19}$ (x = 0.4 and 0.5) nanohexaferrites

Table 1 Elemental composition of $SrCe_xY_yFe_{12-(x+y)}O_{19}$ nanohexaferrites

Symbol	Element	Atomic weight	Mass % (x = y = 0.4)	Mass % (x = y = 0.5)
Sr	Strontium	87.62	7.90	7.82
Ce	Cerium	140.12	5.06	6.25
Y	Yttrium	88.91	3.20	3.97
Fe	Iron	55.85	56.42	54.83
O	Oxygen	16.00	27.42	27.13

relationship with the frequency of the applied field in the *log–log* plots, as described by Jonscher's law of power. In addition, there is an adverse effect on the conductance of both Sr-hexaferrites of the ionic substituents. It can also be noted from the relevant plots that overall conductivity decreases with increasing substitutional rate of both cerium and yttrium (see Fig. 4e, f) [16].

Also consistent with Maxwell–Wagner's two-layer model, cerium and yttrium substituted M-type strontium hexaferrite contain highly conducting grains isolated by grain boundaries with a lower conductivity. Thus, the mobility of the charge carriers increases as the grain size grows (Fig. 5). This may be a possible reason behind the enhanced conduction mechanism. The increase in *ac* conductivity at higher frequencies can be possibly attributed to a trend for a small polaron hopping mechanism [17].

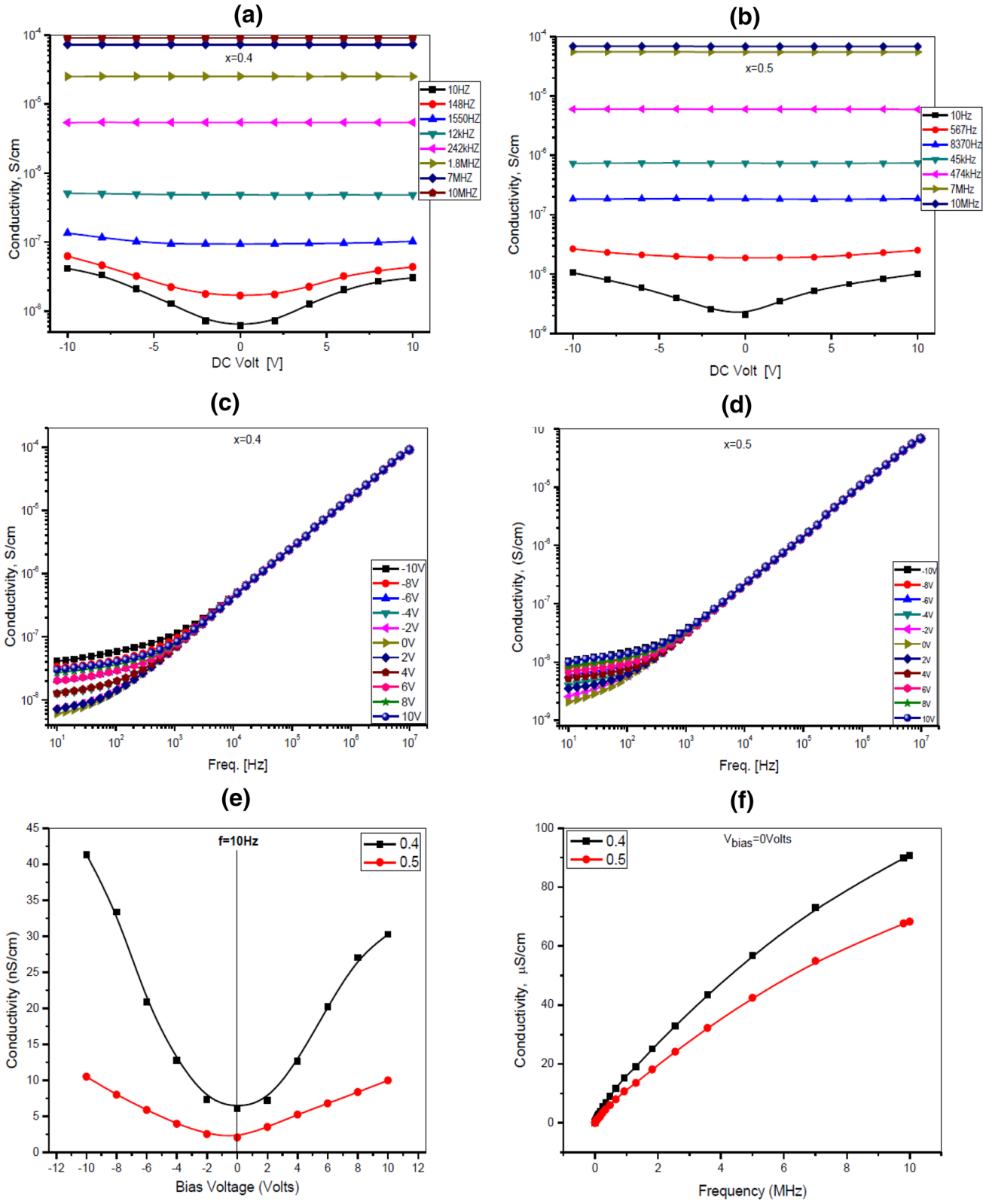

Fig. 4 (i) The conductivities of the $SrY_xCe_xFe_{12-2x}O_{19}$ nanohexaferrites as a function of dc bias potential at various frequencies for the Y and Ce substitutional ratios of **a** 0.4 and **b** 0.5; (ii) conductivity versus frequency at various *dc* bias potentials for both substitution ratios of **c** 0.4 and **d** 0.5; (iii) **e** conductivity versus the dc bias potential at a lowest frequency of 10 Hz for both substitution ratios; (iv) **f** conductivity versus frequency at no-bias condition for both substitutional ratios

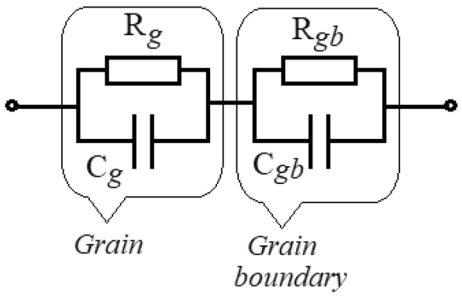

Fig. 5 Equivalent circuitry used to represent the electrical properties of both grain and grain-boundary effects

3.3.1 Complex Impedance and Nyquist Plotting

In case of any substituted hexaferrites, the dielectric behaviour can typically be regulated by the volumetric ratio of grains/grain boundaries. At lower frequencies, the contribution of grain boundaries to conductivity is greater than in grains. Due to the poorer conduction, the motion of the charge carriers decreases at the grain boundary, so grain boundaries become less conductive than grain. When working on Ce- and Y-substituted Sr-hexaferrites, attention has been drawn to a similar characteristic pattern because the grain boundaries are found to be larger than the volumetric grains. This means that grain boundaries in Sr-hexaferrites act as a barrier in conduction mechanism. Yet, the substitution of both cerium and yttrium in Sr-hexaferrites has declined the resistance of their grain boundaries made it comparable to that of grain boundaries of Sr-hexaferrites [18].

As a characteristic evaluation, Nyquist plotting is an important tool to study the effect of ferrite materials on conduction mechanism of both micro and nano structures. The analysis of Nyquist plots provides some significant parameters related to non-Debye relaxation behavior. Figure 6a, b show that the resistance is strongly dependent on the applied *dc* bias potentials while being frequency independent in the high frequency range. On the one hand, while the frequency dependence of the resistance on the substitution rate of both "Ce" and "Y" is quite variable, the frequency dependence in the high frequency region can remain unchanged.

On the other hand, as shown in Fig. 6c, d, reactance values show less deviation under the influence of *dc* bias potentials at low frequency. Both resistance and reactance in a relatively higher frequency region signify some reduction tendencies in the frequency-dependency relevant to exponent power law.

Nyquist plot for cerium and yttrium substituted M-type strontium hexaferrites is depicted in Fig. 6e, f. It can be seen that M-type Sr-hexaferrites demonstrate a single semicircular arc for both substitutions in the *dc* bias potential between − 10 and 10 V. While the substitution ratio of 0.5 of "Ce" and "Y" in the Sr-hexaferrites becomes predominant over the trend of a single semi-circular arc, the substitution ratio of 0.4 indicates that the fewer effect of bias polarity corresponds to the semi-circular arc. As a consequence, the characteristic tendencies of the arc for both substitutional ratios were recorded slightly different from each other.

Fig. 6 (i) **a** Resistance for ratio of 0.4 and **b** resistance for ratio of 0.5, and **c** reactance for ratio of 0.4 and **d** reactance for ratio of 0.5 of the $SrY_xCe_xFe_{12-2x}O_{19}$ nanohexaferrites as a function of frequency for a variety of *dc* bias potentials (ii) the Nyquist plots of $SrY_xCe_xFe_{12-2x}O_{19}$ nanohexaferrites for a variety of *dc* bias potentials in the frequency range from 10 Hz to 10 MHz for substitutional ratios of **e** 0.4 and **f** 0.5

In general, Sr-hexaferrites may contain non-homogeneous granular structures. Thus, a single semicircular arc can originate from many electrically active regions where grain, grain boundaries, as well as electrode polarization effects are caused, and at the same time indicates the presence of the grain interiors of Sr-hexaferrites. At higher frequencies, the semicircular arc can be attributed to grain properties. So, the impedance spectra could be characterised by the presence of a single semicircular arc. There would be some reasonable effects on the emergence of a relevant arc such as grain effects, grain boundary effects and finally grain–grain boundary effects [19]. The other important effect may be based on the types and ratios of substitutions in Sr-hexaferrites. It can be seen from the trend of the curve of Fig. 6 that the resistance is smaller for cereals but larger for grain boundaries. For this reason, it can be assumed that the low-frequency trends in conductivity are the result of the charge polarization on the grain boundaries.

3.4 Permittivity

3.4.1 Dielectric Constant

Figure 7a, b show that the dielectric constant for Sr-hexaferrites changes with frequency under *dc* bias potentials in the low frequency region, while the dielectric constant remains stable for both substitution ratios in the higher frequency region. Figure 7c, d show that the dispersion in the dielectric constant in the low frequency region is recorded for both substitution ratios, as in the medium and high frequency regions. So, the dielectric constant is reduced with increasing frequency in a tendency of a power law, but a *dc* potential independent of a click-through jumping occurring at a frequency of about 200 kHz for both substitutional ratios. In addition, the dielectric constant is reduced by the ratio of the combined cerium and yttrium substitutions, as well as by the potential for elevated *dc* bias ranging from − 10 to 10 V.

For M type Sr-hexaferrites, it is expected that all these characteristic performances are general dielectric actions. Therefore, such situations can be interpreted based on the

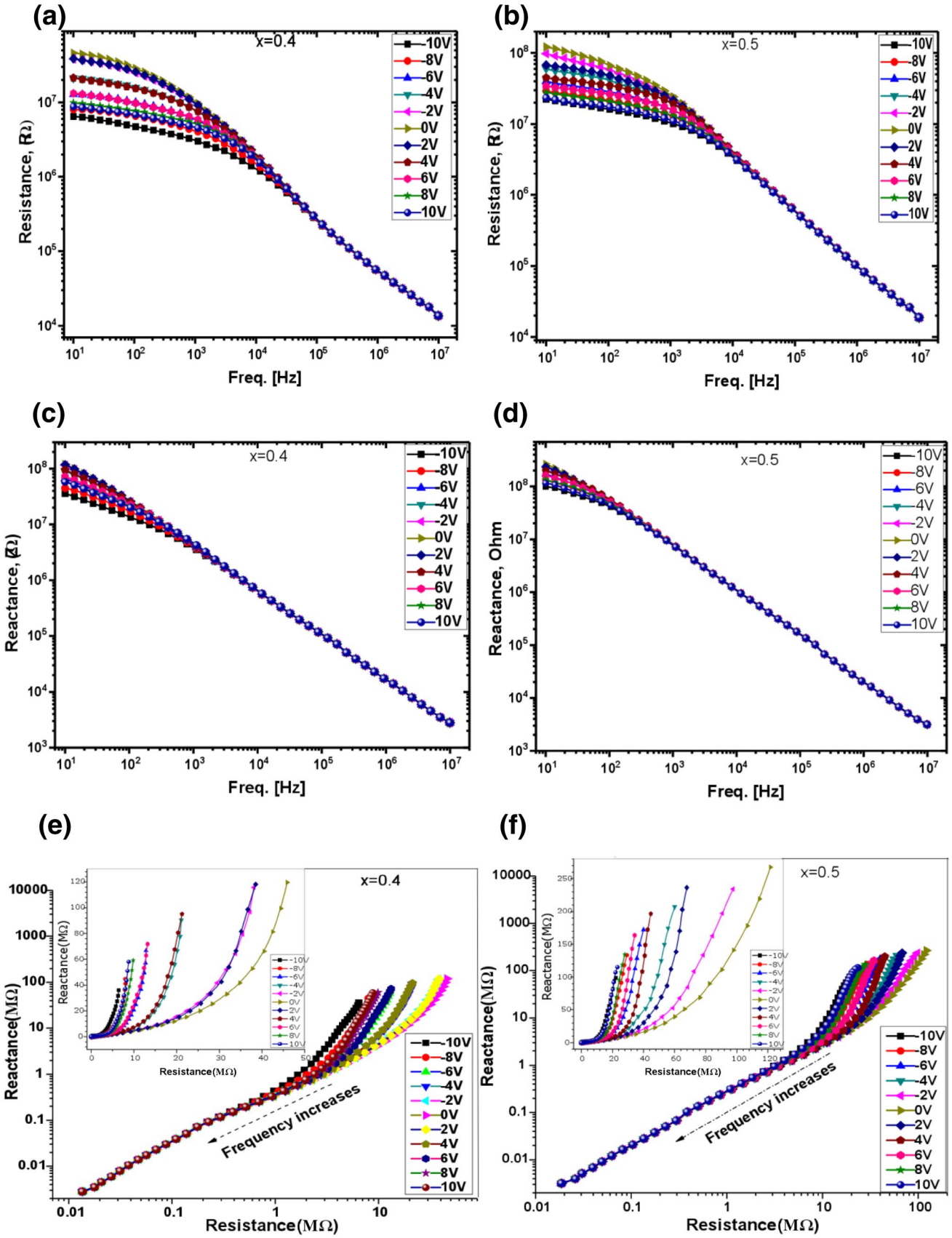
(a)
x=0.4
Resistance, (Ω)
Freq. [Hz]
(b)
x=0.5
Resistance, (Ω)
Freq. [Hz]
(c)
x=0.4
Reactance, (Ω)
Freq. [Hz]
(d)
x=0.5
Reactance, Ohm
Freq. [Hz]
(e)
x=0.4
Reactance(MΩ)
Resistance(MΩ)
Frequency increases
(f)
x=0.5
Reactance(MΩ)
Resistance(MΩ)
Frequency increases
-10V
-8V
-6V
-4V
-2V
0V
2V
4V
6V
8V
10V

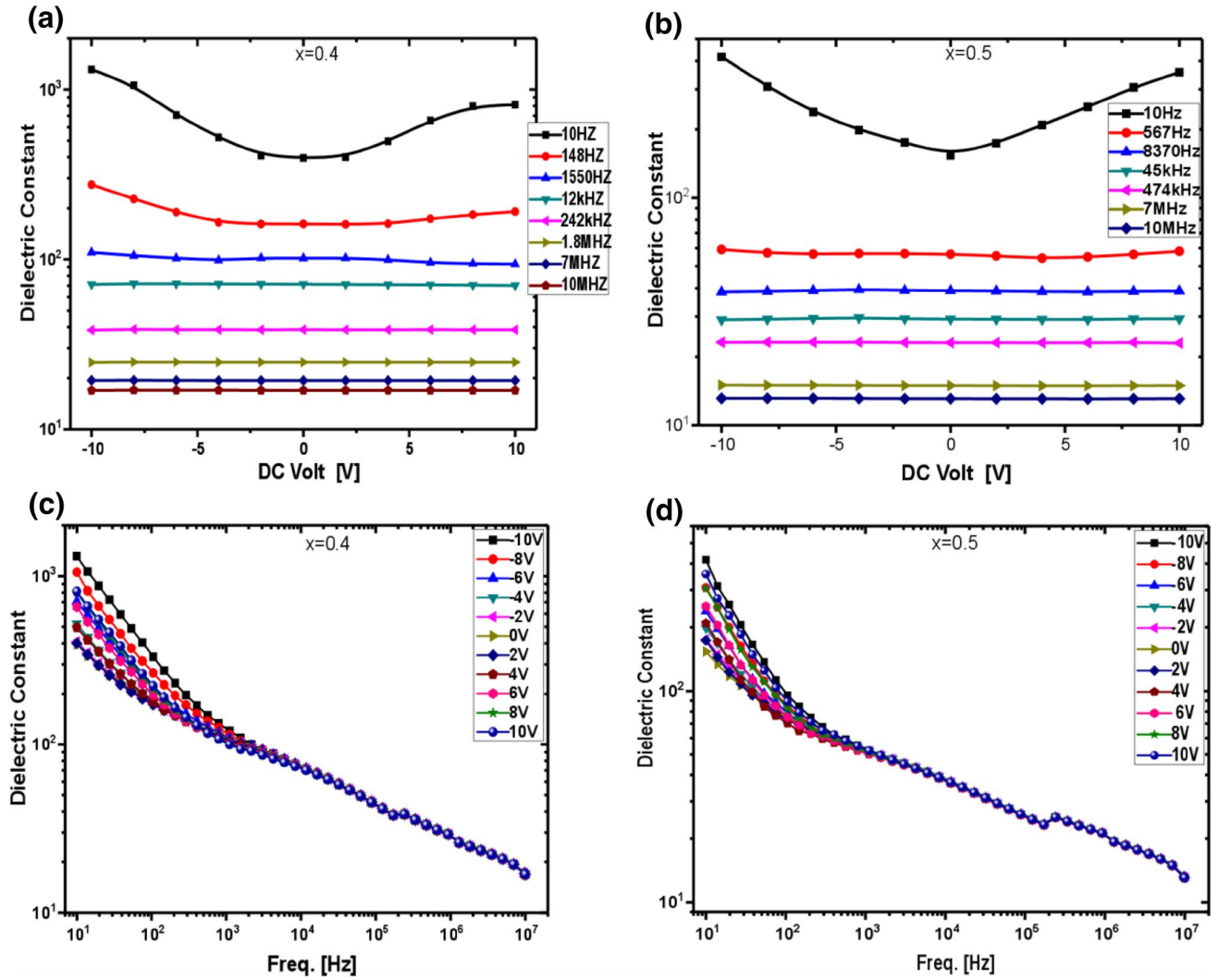

Fig. 7 (i) Dielectric constant of $SrY_xCe_xFe_{12-2x}O_{19}$ nanohexaferrites as function of *dc* bias potentials for a given frequency range for substitutional ratios of **a** 0.4 and **b** 0.5; (ii) dielectric constant versus frequency for a variety of *dc* bias potentials for substitutional ratios of **c** 0.4 and **d** 0.5

basic understanding that the hopping conduction between the ferrous and ferric ions increases at higher frequencies. In fact, some charges released from various trapping centers reinforce the conduction mechanism of the hopping process by electron conduction [5].

Dielectric measurements for both substituted Sr-hexaferrite were obtained between the *dc* biased potentials of − 10 and 10 V in the frequency range of 10 Hz–10 MHz. The dielectric arrangement of Sr-hexaferrites consists of two layers, one of which contains a large number of grains and other layers of grain boundaries that play an important role as highly resistive channels at lower frequencies as described by Maxwell–Wagner model. This is the way that the polarization in the Sr-hexaferrites is similar to the conduction process by the exchange of electrons between ferrous and ferric ions [5]. When the stimulation frequency of the applied electric field is increased, the exchange rate of electrons is far behind the frequency of the excitation speed of the electrons and thus the dielectric constant is decreasing. The increase in *dc* bias potentials, ranging from − 10 to 10 V, causes a drop in the dielectric constant for both of the substitution ratios. It has also been observed that the dielectric constant values are significantly increased at relatively low frequencies. Therefore, it is probably due to moisture, voids, dislocation density and impurities in ferrites. The concentration of ferrous ions is reduced due to the reduction of

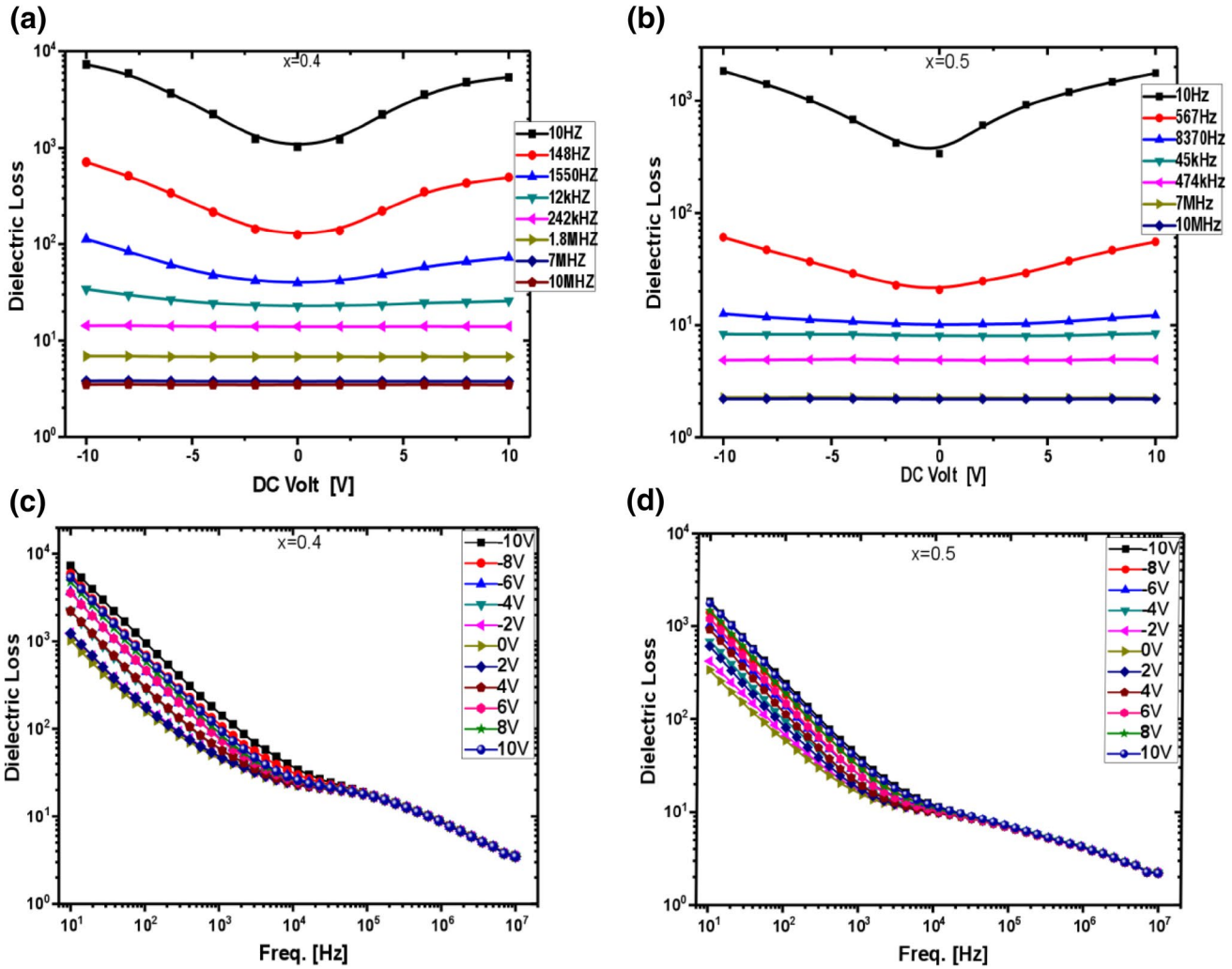

Fig. 8 (i) Dielectric loss of $SrY_xCe_xFe_{12-2x}O_{19}$ nanohexaferrites as function of *dc* bias potentials for a given frequency range for substitutional ratios of **a** 0.4 and **b** 0.5; (ii) dielectric loss versus frequency for a variety of *dc* bias potentials for substitutional ratios of **c** 0.4 and **d** 0.5

the polarisation and hence the dielectric constant. This can be explained by the Koop's model that the dielectric constant at low frequencies is bound to the grain boundaries. These grain boundaries act as highly resistant layers, and thus contribute to a slightly higher dielectric constant. The dielectric constant of the Ce- and Y-substituted M-type Sr-hexaferrites is depicted in Fig. 7 as a function of the frequency at different *dc* bias potentials for both substitution ratios. In the higher bias potential, the more electrons move freely, the more they contribute to the conduction mechanism.

Because the increase in *dc* bias leads to an increase in polarization, the dielectric constant increases with the increase in *dc* bias potential due to high electric field inductions. An increase in the *dc* bias potentials result in a highly activated hopping process for the charge carriers and hence, the dielectric polarization increases and thereby causing a rise in dielectric constant. It is also known that at low frequencies, dipolar and interfacial polarizations play an important role and strongly depend on *dc* bias. At higher frequencies, electronic and ionic polarizations become the main contributors, and therefore, *dc* bias potential dependence can produce insignificant contributions.

As a result, the frequency-dependent variation of the dielectric constant reveals dispersion originating from Maxwell–Wagner-type interface polarization and it is observed that the low frequency dispersion in the Sr-hexaferrites depends on a space-charge effect, and this can be considered to be consistent with the Koop's phenomenological theory.

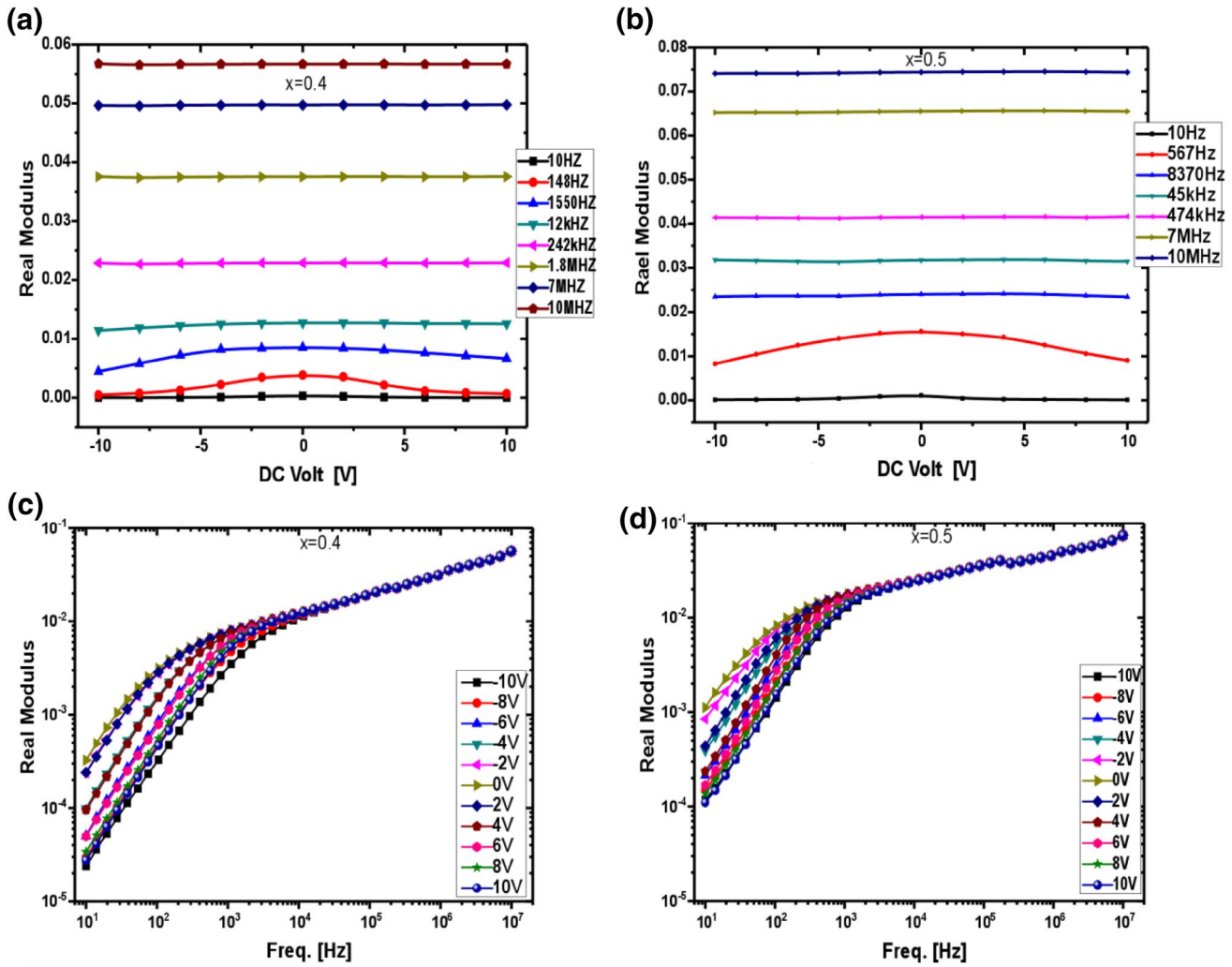

Fig. 9 (i) Dielectric real modulus of $SrY_xCe_xFe_{12-2x}O_{19}$ nanohexaferrites as function of *dc* bias potentials for a given frequency range for substitutional ratios of **a** 0.4 and **b** 0.5; (ii) dielectric real modulus versus frequency for a variety of *dc* bias potentials for substitutional ratios of **c** 0.4 and **d** 0.5

3.4.2 Dielectric Loss

If some of the iron ions migrate to the tetrahedral site from the octahedral region due to occupation with some substitutions of both cerium and yttrium ions, an increase in electrical resistance and a decrease in the value of the dielectric constant and dielectric loss tangent will occur.

The dielectric loss is also determined in terms of tangent loss factor and dielectric constant defined by the following equation;

$$\varepsilon''(\omega;T) = \varepsilon'(\omega;T)\tan\delta$$

Since the dielectric constant and the loss factor are both dependent on frequency and temperature, the substitution types and ratios in Sr-hexaferrites must also be dependent on the same.

Figure 8a, b show that the dielectric loss of Sr-hexaferrites has a slight change under *dc* bias potentials at lower frequencies, while it remains constant for both (Ce and Y) substitutional ratios at higher frequencies (0.4 and 0.5). Figure 8c, d also demonstrate that while the remarkable dispersion in the dielectric loss for both substitutions is observed at low frequencies, the dielectric loss in the medium and high frequency regions is still reduced by increasing frequency as a power law dependency. Thereafter, the dielectric loss drops with an increase in *dc* bias potentials ranging from − 10 to 10 V as it decreases with increasing proportions of both substitutions. This can be attributed to the interface relaxation process. The reason for this is that the Koop's model reveals that Sr-hexaferrites ceramics contain both grains and grain boundaries, such that grains have high conductivity and grain boundaries have lower conductivity. Having a low *dc* bias potential suppresses the effect of grain boundaries,

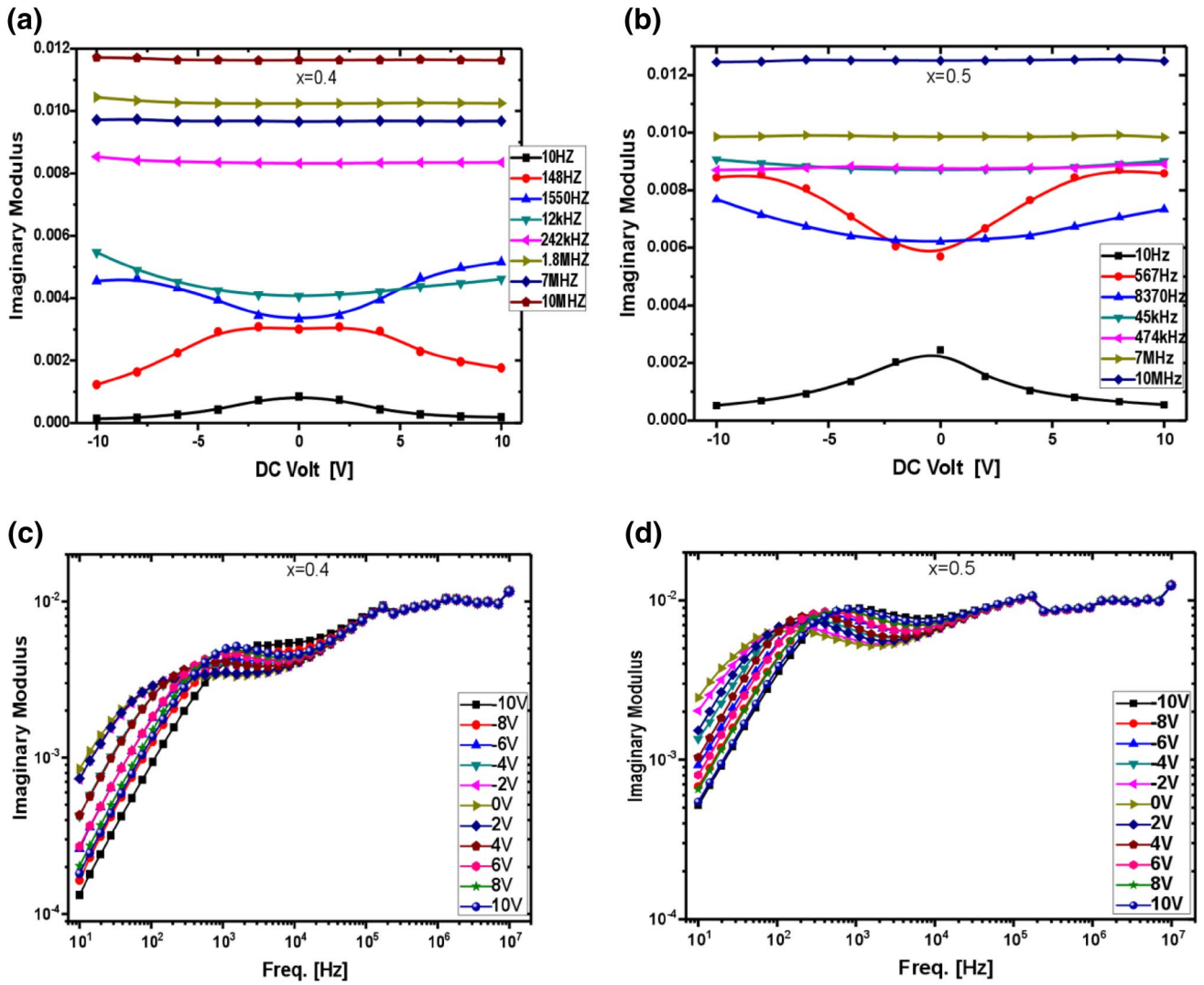

Fig. 10 (i) Dielectric imaginary modulus of $SrY_xCe_xFe_{12-2x}O_{19}$ nanohexaferrites as function of *dc* bias potentials for a given frequency range for substitutional ratios of **a** 0.4 and **b** 0.5; (ii) dielectric imaginary modulus versus frequency for a variety of *dc* bias potentials for substitutional ratios of **c** 0.4 and **d** 0.5

which increases dielectric loss. As the absolute value of the *dc* bias potentials increases, the role of the grains becomes more and more effective and causes a decrease in the dielectric loss. It is also evident in both Figs. 7c, d, and 8c, d that the dielectric loss decreases with an increase in substitution rates similar to the dielectric constant. This can be explained in terms of conduction gains, which are the opposite of dielectric losses. The most important source of conduction loss could be due to the ferrous concentration on octahedral sites. A detailed correlation between the conduction mechanism and the dielectric loss has been extensively studied in terms of the similarity of the charge polarization to the conduction mechanism in the hexaferrites. In the lower frequency region, the dispersion in the dielectric losses is wider than that in the dielectric constant for both substitutions, whereas no dispersion is observed in the higher frequency region. Moreover, the conduction mechanism in ferrites can be explained by a reduction in frequency, so the longer the time required to displace the charge within the grains, the lower the conduction and the higher the dielectric losses. As the stimulation frequency increases, the conduction electrons do not have enough time to follow the frequency of the applied electric field, so that the conduction within the grain is reduced and therefore the scattering factor is reduced. This may be due mainly to the modification in ferrous ion concentration caused by the substitution ions on octahedral sites.

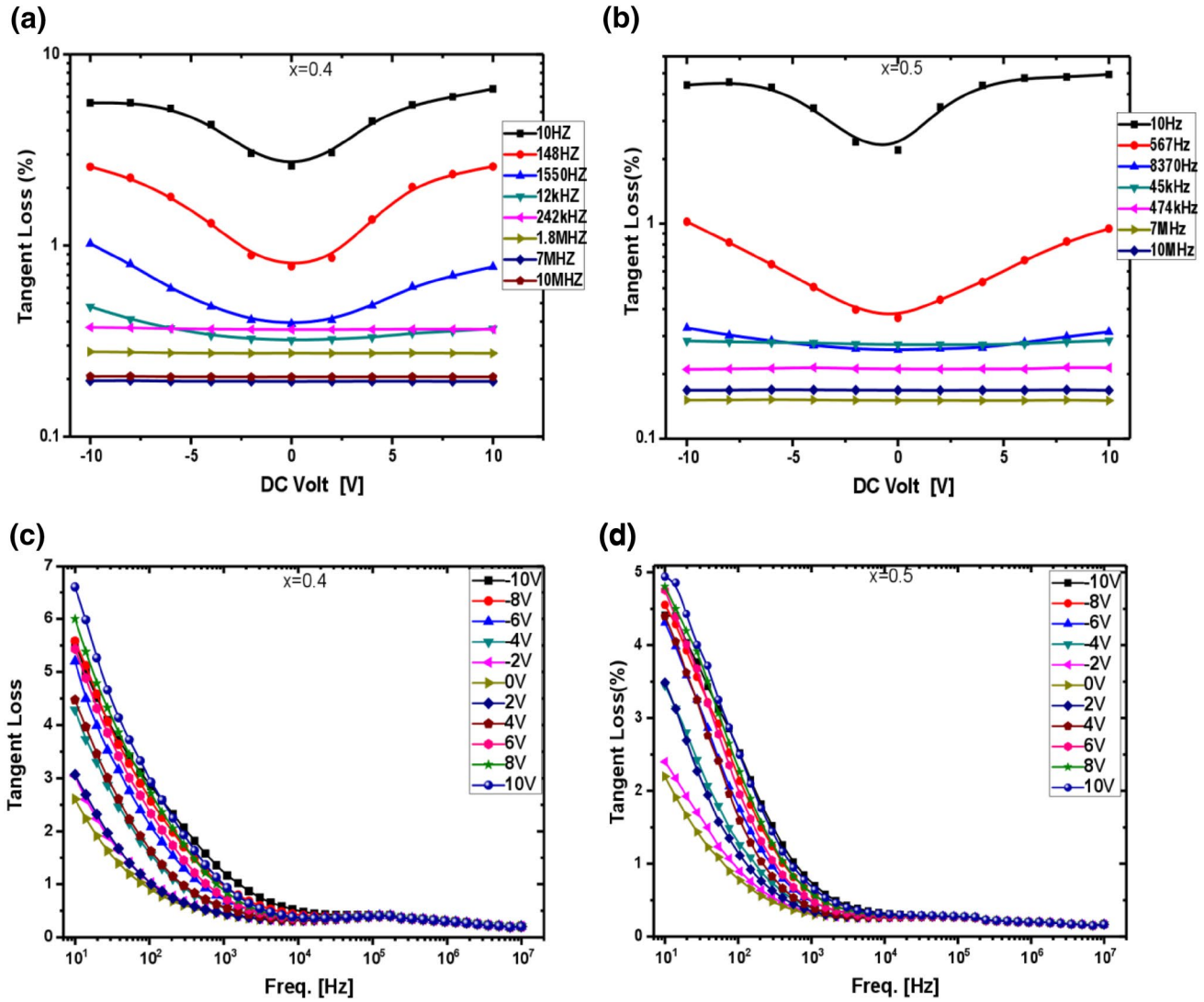

Fig. 11 (i) Dielectric tangent loss of $SrY_xCe_xFe_{12-2x}O_{19}$ nanohexaferrites as function of *dc* bias potentials for a given frequency range for substitutional ratios of **a** 0.4 and **b** 0.5; (ii) dielectric tangent loss versus frequency for a variety of *dc* bias potentials for substitutional ratios of **c** 0.4 and **d** 0.5

3.4.3 Dielectric Modulus

It is important to note that the complex electric module may be an important effective tool for analyzing the dielectric properties of dielectric materials, as well as the conduction mechanism, due to electrode polarization. Hence, the dielectric module can be evaluated by dividing it into real and imaginary components of complex dielectric data including the dielectric constant ε' and dielectric loss ε'' parameters, and then expressed in the following form [20, 21].

$$M^*(\omega) = \frac{1}{\varepsilon^*} = M'(\omega) + iM''(\omega) = \frac{\varepsilon' + i\varepsilon''}{\varepsilon''^2 + \varepsilon''^2}$$

where M' and M'' is the real and complex component of complex dielectric modulus, respectively.

3.4.3.1 Real Modulus The real parts of the dielectric modulus of both substituted Sr-hexaferrites are shown as a function of the *dc* bias potential in Fig. 9a, b for both substitution ratios in the frequency range of up to 10 MHz. Once again, the real modulus as the frequency function of the same samples is depicted in Fig. 9c, d for various *dc* bias potentials for the same substitution ratios. At low and high frequencies, the real modulus remains nearly constant when the bias potential changes from − 10 to 10 V, because only at moderate frequencies it is reduced by an absolute *dc* bias potential. In addition, since no propagation is recorded at high frequencies, the dispersion in the real modulus occurs for a

dc bias variation. However, in a lower frequency region the dispersion is limited when substitutional ratio is increased. It can also be seen in Fig. 9 that the two relaxation zones can be interpreted in the measured frequency range. Therefore, on the lower frequency side it represents the dispersive attitude of which charge carriers can perform some promising hopping sites among ferrous and ferric ions.

3.4.3.2 Imaginary Modulus The frequency-dependent dielectric imaginary modulus of both substituted Sr-hexaferrite is shown in Fig. 10a, b for each substitutional ratio as a function of *dc* bias potentials. Furthermore, the imaginary modulus of the same samples as a function of frequency is illustrated in Fig. 10c, d for a variety of *dc* bias potentials for the same substitutional ratios. The imaginary modulus at frequencies below 30 kHz is observed to fluctuate slightly for various frequencies, except for substitutional ratios, as the bias potential varies from values of − 10 to 10 V. However, the imaginary modulus at frequencies above 30 kHz remains almost constant except for a jump click with a certain frequency of about 200 kHz.

Moreover, since a lesser dispersion is recorded at medium frequencies, a slight dispersion occurs in the imaginary mode for a variety of *dc* bias potentials. However, when the initial substitution rate is raised to 0.5, it fluctuates with increasing frequency in the medium and high frequency region. Such trends in Sr-hexaferrite ceramics provide more information about the mechanism of hopping-type-mechanism depending on the *dc* bias potential relationship on the *ac* electric field for conduction, especially at certain frequencies such as 10 Hz (for both ratios of 0.4 and 0.5) and 148 Hz (a ratio of only 0.4). It can be noticed that the imaginary modulus, which is a sign of energy loss in the electric field, increases rapidly with the frequency in the grain core region. As a result, the peak value at medium frequencies around 0.5–0.8 kHz for both substitutions could be indicative of the conduction from long range to short range mobility with an increase in frequency.

3.4.4 Tangent Loss: Dissipation Factor

The dielectric tangent loss of $SrY_xCe_xFe_{12-2x}O_{19}$ nanohexaferrites (x = 0.4 and 0.5) as function of *dc* bias potentials is shown in Fig. 11a, b at various frequencies for both substitutional ratios. Once again, the tangent loss of the same samples as a function of frequency is depicted in Fig. 11c, d for a variety of *dc* bias potentials for both substitutional ratios, respectively. At lower frequencies of up to 10 kHz, the tangent loss changes with respect to the *dc* bias potential, while at high frequencies it remains almost constant.

Additionally, a remarkable dispersion in tangent loss occurs for some variation of *dc* biased potentials since lesser dispersion is recorded at higher frequencies. However, dissipation factor decreases with increasing frequency in low and medium frequency regions while tangent loss for both substitutions remains constant. As the substitution rate increased to 0.5, it was found that the value of tangential loss decreased. Such trends in the loss factor can be elucidated with the help of Koop's model, which states that Sr-hexaferrites contain both grains and grain boundaries; so that the grains have a high conductivity and the grain boundaries have low conductivity as previously mentioned. At a low bias potential, the effect of grain boundaries, which reduces the loss of tangent, is overwhelmed. As the absolute value of *dc* bias potentials increases, the role of grains becomes more and more effective and leads to increased tangential loss.

It can be explained that the space charge is dominated by the presence of free charges on grain boundaries, which is an important parameter at lower frequencies. Thus, the narrower the grain boundaries, the greater the dielectric constant. It is an observable fact that electron exchange between ferrous and ferric ions cannot track the alteration direction of the externally-applied field beyond a certain frequency. Consequently, space charge polarization has some contribution to the total polarization in nanohexaferrites. Moreover, hopping exchange of charge carriers between two localized states is ruled out by the localized density of states as well as subsequent displacement of these charges via externally-stimulating field [22].

4 Conclusion

Structural and dielectric properties of synthesized Ce and Y substituted $SrFe_{12}O_{19}$ (x = 0.4 and 0.5) were studied in details. It has been demonstrated that the dielectric losses in Sr-hexaferrites are mainly due to conduction mechanism caused by space charge polarization. As the stimulation frequency increases, the charge carriers between the ferrous and ferric ions will not have enough time to trace the alternative electric field. As a result, the polarization is reduced and hence dielectric loss decreases. Dielectric constant, dielectric loss, and dielectric loss tangent all decay exponentially in a lower frequency range, but decline in proportion to the power law in the higher frequency range. The reduction of tangential loss by increasing frequency can be assigned to the Maxwell–Wagner polarization and conduction mechanism. Consequently, relaxation tendencies can be interpreted by considering modulus formalism.

Acknowledgements Dr. A. Baykal thanks the Deanship of Scientific Research (DSR) and Institute for Research and Medical Consultations (IRMC) of Imam Abdulrahman Bin Faisal University for supporting this study. Dr. Munirah is grateful to the Core Lab teams of King Abdullah University of Science and Technology (KAUST) for providing the required analysis.

References

1. K. Miura, M. Masuda, M. Itoh, T. Horikawa, K. Machida, Microwave absorption properties of the nano-composite powders recovered from Nd–Fe–B bonded magnet scraps. J. Alloys Compd. **408–412**, 1391 (2006)
2. F.M.M. Pereira, M.R.P. Santos, R.S.T.M. Sohn, J.S. Almeida, A.M.L. Medeiros, M.M. Costa, A.S.B. Sombra, Magnetic and dielectric properties of the M-type barium strontium hexaferrite ($Ba_xSr_{1-x}Fe_{12}O_{19}$) in the RF and microwave (MW) frequency range. J. Mater. Sci.: Mater. Electron. **20**, 408 (2009)
3. P. Kaur, S.K. Chawla, S.S. Meena, S.M. Yusuf, K. Pubby, S.B. Narang, Modulation of physico-chemical, magnetic, microwave and electromagnetic properties of nanocrystalline strontium hexaferrite by Co–Zr doping synthesized using citrate precursor sol-gel method. Ceram. Int. **43**, 590–598 (2017)
4. R.K. Mudsainiyan, S.K. Chawla, S.S. Meena, N. Sharma, R. Singh, A. Das, Cations distribution and magnetic properties of Co–Zr doped $BaCo_xZr_xFe_{(12-2x)}O_{19}$ prepared via citrate precursor sol-gel route. Ceram. Int. **40**, 16617 (2014)
5. Y. Bakış, I.A. Auwal, B. Ünal, A. Baykal, Conductivity and dielectric properties of $SrLa_xBi_xY_xFe_{12-3x}O_{19}$ ($0.0 \leq x \leq 0.33$) hexaferrites. Ceram. Int. **42**, 11780 (2016)
6. Y. Bakış, I.A. Auwal, B. Ünal, A. Baykal, Maxwell-Wagner relaxation in grain boundary of $BaBi_xLa_xY_xFe_{12-3x}O_{19}$ ($0.0 \leq x \leq 0.33$) hexaferrites. Composites B **99**, 248 (2016)
7. D. Seifert, J. Töpfer, F. Langenhorst, J.-M. Le Breton, H. Chiron, L. Lechevallier, Synthesis and magnetic properties of La-substituted M-type Sr hexaferrites. J. Magn. Magn. Mater. **321**, 4045 (2009)
8. Z. Mosleh, P. Kameli, A. Poorbaferani, M. Ranjbar, H. Salamati, Structural, magnetic and microwave absorption properties of Ce-doped barium hexaferrite. J. Magn. Magn. Mater. **397**, 101 (2016)
9. B.H. Bhat, B. Want, Dielectric and impedance behavior of neodymium substituted strontium hexaferrite. Appl. Phys. A **122**, 148 (2016)
10. L. Peng, L.Z. Li, R. Wang, Y. Hu, X.Q. Tu, X.X. Zhong, Effect of La–CO substitution on the crystal structure and magnetic properties of low temperature sintered $Sr_{1-x}La_xFe_{12-x}Co_xO_{19}$ ($x = 0$–0.5) ferrites. J. Magn. Magn. Mater. **393**, 399 (2015)
11. P. Shen, J.H. Luo, Y. Zuo, Z. Yan, K. Zhang, Effect of La-Ni substitution on structural, magnetic and microwave absorption properties of barium ferrite. Ceram. Int. **43**, 4846 (2017)
12. Z.Y. Zhang, X.X. Liu, X.J. Wang, Y. Peng, R. Li, Effect of Nd–Co substitution on magnetic and microwave absorption properties of $SrFe_{12}O_{19}$ hexaferrites. J. Alloys Compd. **525**, 114 (2012)
13. Z.F. Zi, Q.C. Liu, J.M. Di, Y.P. Sun, Effects of Ce–Co substitution on the magnetic properties of M-type barium hexaferrites. Solid State Commun. **152**, 894 (2012)
14. M.N. Ashiq, S. Shakoor, M. Najam-ul-Haq, M.F. Warsi, I. Ali, I. Shakir, Structural, electrical, dielectric and magnetic properties of Gd–Sn substituted Sr-hexaferrite synthesized by sol–gel combustion method. J. Magn. Magn. Mater. **374**, 173 (2015)
15. M.A. Almessiere, Y. Slimani, H.S. El Sayed, A. Baykal, Structural and magnetic properties of Ce-Y substituted strontium nanohexaferrites. Ceram. Int. **44**, 12511 (2018)
16. R.A. Nandotaria, R.B. Jotaniaa, C.S. Sandhub, M. Hashimc, S.S. Meenad, P. Bhattd, S.E. Shirsath, Magnetic interactions and dielectric dispersion in Mg substituted M-type Sr–Cu hexaferrite nanoparticles prepared using one step solvent free synthesis technique. Ceram. Int. **44**, 4426 (2018)
17. K. Chahal, K.S. Samra, Magnetic and dielectric behaviour of praseodymium substituted barium hexaferrite. J. Alloys Compd. **737**, 387 (2018)
18. B. Want, B.H. Bhat, B.Z. Ahmad, Effect of lanthanum substitution on dielectric relaxation, impedance response, conducting and magnetic properties of strontium hexaferrite. J. Alloys Compd. **627**, 78 (2015)
19. J. Liu, C.C. Duan, W.G. Yin, W.N. Mei, R.W. Smith, J.R. Hardy, Large dielectric constant and Mawwell-Wagner relaxation in $Bi_{2/3}Cu_3Ti_4O_{12}$. Phys. Rev. B **70**, 144106 (2004)
20. H. Sözeri, A. Baykal, B. Ünal, Low temperature synthesis of single domain Sr-hexaferrite particles by solid state reaction route, Phys. Status Solidi A **209**, 2002 (2012)
21. A. Baykal, M. Demir, B. Ünal, H. Sözeri, M.S. Toprak, Synthesis, characterization, and dielectric properties of $BaFe_{10}(Mn^{2+}Zn^{2+}Zn^{2+})O_{19}$ hexaferrite. J. Supercond. Nov. Magn. **29**, 199 (2016)
22. K. Praveena, M. Bououdina, M.P. Reddy, S. Srinath, R. Sandhya, S. Katlakunta, Structural, magnetic, and electrical properties of microwave-sintered Cr^{3+}-doped Sr hexaferrites. J. Electron. Mater. **44**, 524 (2015)